

Supersymmetric top and bottom squark production at hadron colliders

Wim Beenakker

*Theoretical High Energy Physics, IMAPP, Radboud University Nijmegen,
P.O. Box 9010, NL-6500 GL Nijmegen, The Netherlands*

Silja Breusling

*Institut für Theoretische Teilchenphysik und Kosmologie, RWTH Aachen University,
D-52056 Aachen, Germany
Nikhef Theory Group, Science Park 105, 1098 XG Amsterdam, The Netherlands*

Michael Krämer

*CERN, Physics Department, Theory Unit, CH-1211 Geneva 23, Switzerland
Institut für Theoretische Teilchenphysik und Kosmologie, RWTH Aachen University,
D-52056 Aachen, Germany*

Anna Kulesza

*Institut für Theoretische Teilchenphysik und Kosmologie, RWTH Aachen University,
D-52056 Aachen, Germany*

Eric Laenen

*ITFA, University of Amsterdam, Science Park 904, 1018 XE Amsterdam,
ITF, Utrecht University, Leuvenlaan 4, 3584 CE Utrecht,
Nikhef Theory Group, Science Park 105, 1098 XG Amsterdam, The Netherlands*

Irene Niessen

*Theoretical High Energy Physics, IMAPP, Radboud University Nijmegen,
P.O. Box 9010, NL-6500 GL Nijmegen, The Netherlands*

ABSTRACT: The scalar partners of top and bottom quarks are expected to be the lightest squarks in supersymmetric theories, with potentially large cross sections at hadron colliders. We present predictions for the production of top and bottom squarks at the Tevatron and the LHC, including next-to-leading order corrections in supersymmetric QCD and the resummation of soft gluon emission at next-to-leading-logarithmic accuracy. We discuss the impact of the higher-order corrections on total cross sections and transverse-momentum distributions, and provide an estimate of the theoretical uncertainty due to scale variation and the parton distribution functions.

KEYWORDS: QCD, Supersymmetry, resummation.

Contents

1. Introduction	1
2. Stop and sbottom pair production	3
2.1 Threshold resummation for the total inclusive cross section	5
2.2 Threshold resummation for the transverse-momentum distribution	7
3. Numerical results	9
3.1 Results for the total cross section	10
3.2 Results for the transverse-momentum distribution	12
4. Conclusions	13
A. SUSY parameter dependence of stop and sbottom cross sections	23

1. Introduction

The search for supersymmetry [1, 2] is a central part of the physics program at the proton–antiproton collider Tevatron with a centre-of-mass energy of $\sqrt{S} = 1.96$ TeV and at the proton–proton collider LHC, which started operation in 2010 at $\sqrt{S} = 7$ TeV. In particular squarks and gluinos, the coloured supersymmetric particles, may be produced copiously in hadronic collisions. The hadroproduction of top squarks (stops) [3] is an important special case, since the strong Yukawa coupling between top quarks, stops and Higgs fields gives rise to potentially large mixing effects and mass splitting [4]. The same holds, albeit to a lesser extent, for bottom squarks (sbottoms). Moreover, if the scalar masses in unified supersymmetric theories are evolved from universal values at high scales down to low scales, the lighter of the stop mass eigenstates is generally driven to the lowest value in the entire squark mass spectrum. The search for the lightest stop therefore plays a special role in the quest to find signals of supersymmetry at hadron colliders.

Searches at LEP [5, 6] and the Tevatron [7]–[11] have placed lower limits on the lighter stop and sbottom mass eigenstates in the range between about 70–200 GeV, depending on the choice of supersymmetric parameters. The LHC will extend the range of sensitivity into the TeV-region [12, 13].

In the minimal supersymmetric extension of the Standard Model (MSSM) [14, 15] with R-parity conservation, stops are pair-produced at hadron colliders:

$$pp/p\bar{p} \rightarrow \tilde{t}_1\bar{\tilde{t}}_1 + X \quad \text{and} \quad \tilde{t}_2\bar{\tilde{t}}_2 + X, \quad (1.1)$$

where \tilde{t}_1 and \tilde{t}_2 denote the lighter and heavier mass eigenstate, respectively. The hadroproduction of mixed $\tilde{t}_1\tilde{\bar{t}}_2$ or $\tilde{t}_2\tilde{\bar{t}}_1$ final states is strongly suppressed since it can only proceed through electroweak channels or QCD-induced loop diagrams [3, 16, 17]. Sbottom hadroproduction is described in a completely analogous manner, so we will focus our discussion on stops. We will, however, comment on potential differences between stop and sbottom hadroproduction, and provide benchmark cross sections for sbottom production at the Tevatron and the LHC.

Accurate theoretical predictions for the stop-pair cross sections are crucial to derive exclusion limits [7]–[11] and, in the case of discovery, can be used to determine the stop masses and properties (see e.g. Refs. [18, 19, 20]). The cross sections for the stop-pair production processes (1.1) have been calculated at next-to-leading order (NLO) in supersymmetric QCD (SUSY-QCD) [3]. The SUSY-QCD corrections significantly reduce the renormalization- and factorization-scale dependence and increase the cross section with respect to the leading-order (LO) predictions if the renormalization and factorization scales are chosen close to the stop mass. Electroweak corrections have been calculated as well [21, 22]. Although they can be sizeable at large invariant masses and large transverse momenta, they are moderate for the inclusive stop cross section. The SUSY-QCD calculation of Ref. [3] has been implemented in the public computer code `Prospino` [23] and presently forms the theoretical basis for the stop mass limits obtained at the Tevatron.

A significant part of the large NLO SUSY-QCD corrections to squark hadroproduction can in general be attributed to the threshold region [24, 3] where the partonic centre-of-mass energy is close to the kinematic threshold for producing massive particles. In this region the NLO corrections are dominated by contributions from soft gluon emission off the coloured particles in the initial and final state and by Coulomb corrections due to the exchange of gluons between the massive particles in the final state. The soft-gluon corrections can be taken into account to all orders in perturbation theory by means of threshold resummation. A considerable amount of work has recently been devoted to the calculation of threshold logarithms for total gluino and squark cross sections [25]–[30]. Final-state stops are excluded in these calculations and all other squark flavours, the so-called light-flavour squarks, are treated as being mass degenerate, neglecting possible mixing effects.

In this work, we extend the previous analyses of threshold resummation for the hadroproduction of gluinos and mass-degenerate light-flavour squarks at next-to-leading logarithmic (NLL) accuracy [25, 27, 30]. Firstly, we consider the hadroproduction of stops and non-mass-degenerate sbottoms. Secondly, we study the impact of NLO and NLL corrections on the transverse-momentum distributions. Since theoretical predictions for differential distributions are input to the experimental analyses, it is important to assess how the shape of the distributions is affected by higher-order corrections. The threshold resummation for transverse-momentum distributions has been studied extensively for Standard-Model processes, see e.g. Refs. [31]–[37], but not yet for SUSY processes.

The paper is structured as follows. In section 2 we review the basic features of stop and sbottom hadroproduction, and we briefly discuss the application of threshold resummation to the transverse-momentum distribution. Section 2 also contains the specific stop-pair

formulae that enter the calculation of the resummed cross sections. State-of-the-art SUSY-QCD predictions for stop hadroproduction at the Tevatron and the LHC, including NLO corrections and NLL threshold resummation, are presented in section 3. We discuss the impact of the NLO+NLL corrections on total cross sections and transverse-momentum distributions and provide an estimate of the theoretical uncertainty due to scale variation and the parton distribution functions. We conclude in section 4. The dependence of the stop and sbottom cross sections on the choice of supersymmetric parameters can be found in the appendix, where also some predictions for specific benchmark scenarios are given.

2. Stop and sbottom pair production

Let us first review some basic features of the stop and sbottom pair-production cross sections. At LO the hadroproduction of stop pairs proceeds through quark-antiquark annihilation and gluon-gluon fusion:

$$\begin{aligned} q\bar{q} &\rightarrow \tilde{t}_1\tilde{\bar{t}}_1 \quad \text{and} \quad \tilde{t}_2\tilde{\bar{t}}_2, \\ gg &\rightarrow \tilde{t}_1\tilde{\bar{t}}_1 \quad \text{and} \quad \tilde{t}_2\tilde{\bar{t}}_2. \end{aligned} \quad (2.1)$$

The corresponding Feynman diagrams are shown in Fig. 1. In contrast to the hadropro-

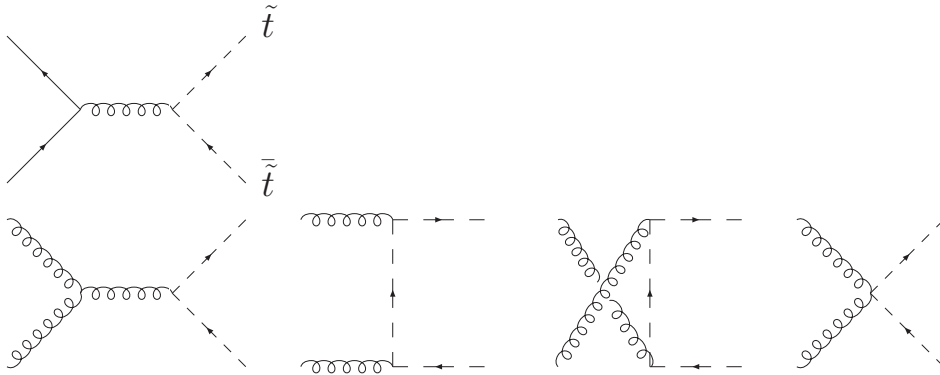


Figure 1: Leading-order Feynman diagrams for the production of stop pairs through quark-antiquark annihilation (first line) and gluon-gluon fusion (second line).

duction of light-flavour squarks, no t -channel gluino-exchange graph occurs in the quark-antiquark channel. In such a t -channel graph the initial-state quarks should have the same flavour as the final-state squarks, but since top quarks are excluded as initial-state partons, the gluino-exchange graph is absent.

The mass eigenstates \tilde{t}_1 and \tilde{t}_2 are related to the weak interaction eigenstates \tilde{t}_L and \tilde{t}_R through mixing: $\tilde{t}_1 = \tilde{t}_L \cos \theta_{\tilde{t}} + \tilde{t}_R \sin \theta_{\tilde{t}}$ and $\tilde{t}_2 = -\tilde{t}_L \sin \theta_{\tilde{t}} + \tilde{t}_R \cos \theta_{\tilde{t}}$. The masses $m_{\tilde{t}_1}$, $m_{\tilde{t}_2}$ and the mixing angle $\theta_{\tilde{t}}$ are obtained from diagonalizing the stop mass matrix and are determined by Standard-Model and soft-supersymmetry-breaking parameters [4]. As mentioned in the introduction, mixed pairs $\tilde{t}_1\tilde{\bar{t}}_2$ or $\tilde{t}_2\tilde{\bar{t}}_1$ cannot be produced in lowest order QCD since the $g\tilde{t}\tilde{\bar{t}}$ and $gg\tilde{t}\tilde{\bar{t}}$ vertices are diagonal in the chiral and in the mass basis.

The description of sbottom hadroproduction $pp/p\bar{p} \rightarrow \tilde{b}_1\tilde{b}_1$ and $\tilde{b}_2\tilde{b}_2$ is completely analogous to that of stop production. The only differences occur in the $b\bar{b} \rightarrow \tilde{b}\tilde{b}$ channel, where the initial-state bottom quarks do allow a t -channel gluino-exchange graph that gives rise to extra contributions. As will be discussed below, these contributions lead to a less-suppressed LO threshold behaviour than the s -channel gluon-exchange contributions. However, we shall demonstrate in the appendix that their numerical impact on the hadronic cross sections is negligible. Thus, for all practical purposes, the LO and higher-order cross-section predictions obtained for stop-pair production apply also to sbottom-pair production if the input parameters, i.e. masses and mixing angles, are modified accordingly.

When decomposed into s -channel colour states, the LO partonic cross sections for the subprocesses (2.1) read in generic notation:

$$\sigma_{q\bar{q} \rightarrow \tilde{t}\tilde{t}, \mathbf{1}}^{(0)} = 0, \quad (2.2)$$

$$\sigma_{q\bar{q} \rightarrow \tilde{t}\tilde{t}, \mathbf{8}}^{(0)} = \frac{\alpha_s^2 \pi (N_c^2 - 1)}{12 N_c^2 s} \beta^3, \quad (2.3)$$

$$\sigma_{gg \rightarrow \tilde{t}\tilde{t}, \mathbf{1}}^{(0)} = \frac{\alpha_s^2 \pi}{N_c (N_c^2 - 1) s} \left[\left(\frac{1}{2} + \frac{2m^2}{s} \right) \beta + \left(\frac{2m^2}{s} - \frac{4m^4}{s^2} \right) \log \left(\frac{1 - \beta}{1 + \beta} \right) \right], \quad (2.4)$$

$$\begin{aligned} \sigma_{gg \rightarrow \tilde{t}\tilde{t}, \mathbf{8}}^{(0)} &= \frac{N_c^2 - 4}{2} \sigma_{gg \rightarrow \tilde{t}\tilde{t}, \mathbf{1}}^{(0)} \\ &+ \frac{\alpha_s^2 \pi N_c}{(N_c^2 - 1) s} \left[\left(\frac{1}{12} + \frac{8m^2}{3s} \right) \beta + \left(\frac{m^2}{s} + \frac{2m^4}{s^2} \right) \log \left(\frac{1 - \beta}{1 + \beta} \right) \right], \end{aligned} \quad (2.5)$$

where α_s is the strong coupling, s the invariant partonic energy and N_c the number of colours. The colour labels $\mathbf{1}$ and $\mathbf{8}$ refer to the familiar singlet and octet colour states in SU(3), but all analytic results in this paper are derived for a general SU(N_c)-theory in order to make the colour structure more transparent. Also note that we use a generic notation for the final-state particles and the associated kinematics: \tilde{t} can be either of the two stop mass eigenstates, with m being the corresponding mass and $\beta = \sqrt{1 - 4m^2/s}$ the corresponding velocity.

The expressions (2.4) and (2.5) for the gluon-gluon fusion cross section agree with the corresponding expression for light-flavour squark production, cf. Ref. [24]. However, the quark-antiquark annihilation contribution (2.3) is different due to the absence of the t -channel gluino-exchange graph. As a consequence, the LO cross section for $q\bar{q} \rightarrow \tilde{t}\tilde{t}$ proceeds through s -channel gluon exchange only and is proportional to β^3 , as opposed to β for other squark flavours. This β^3 behaviour is the combined effect of the standard phase-space suppression factor β and an additional P -wave suppression $\propto \beta^2$ near threshold: the pair of scalar particles needs to be produced in a P -wave state to balance the spin of the intermediate gluon.

Note that the LO cross sections (2.2)–(2.5) only depend on the mass m of the produced stops and not on any other supersymmetric parameters. At NLO, however, the stop mixing angle $\theta_{\tilde{t}}$ enters through corrections involving the $t\tilde{t}\tilde{g}$ vertex and the four-squark couplings. As a result, already the analytical expressions for the $\tilde{t}_1\tilde{t}_1$ and $\tilde{t}_2\tilde{t}_2$ NLO cross sections

are different. Furthermore, virtual corrections involving squark and gluino loops introduce a dependence of the stop-pair cross section on the masses of the squarks and the gluino. The dependence on all these other supersymmetric parameters turns out to be mild, as illustrated in the appendix.

In the threshold region the NLO stop-pair cross section is dominated by soft gluon emission, which leads to corrections $\propto \log^i \beta$ ($i = 1, 2$), and Coulomb corrections $\propto 1/\beta$. In the notation of Ref. [3] the threshold behaviour of the total NLO cross sections reads¹:

$$\begin{aligned} \sigma_{q\bar{q} \rightarrow t\bar{t}}^{(1,\text{thr})} = & \frac{\pi\alpha_s^2(\mu^2)}{48m^2} \frac{N_c^2 - 1}{N_c^2} \beta^3 \left(1 + 4\pi\alpha_s(\mu^2) \left\{ \frac{2C_F - C_A}{16\beta} - \frac{C_A}{4\pi^2} \log(8\beta^2) \right. \right. \\ & \left. \left. + \frac{2C_F}{4\pi^2} \left[\log^2(8\beta^2) - \frac{16}{3} \log(8\beta^2) - \log(8\beta^2) \log\left(\frac{\mu^2}{m^2}\right) \right] \right\} \right) \end{aligned} \quad (2.6)$$

and

$$\begin{aligned} \sigma_{gg \rightarrow t\bar{t}}^{(1,\text{thr})} = & \frac{\pi\alpha_s^2(\mu^2)}{16m^2} \frac{N_c^2 - 2}{N_c(N_c - 1)} \beta \left(1 + 4\pi\alpha_s(\mu^2) \left\{ \frac{2C_F - \frac{N_c^2 - 4}{N_c^2 - 2} C_A}{16\beta} - \frac{N_c^2 - 4}{N_c^2 - 2} \frac{C_A}{4\pi^2} \log(8\beta^2) \right. \right. \\ & \left. \left. + \frac{2C_A}{4\pi^2} \left[\log^2(8\beta^2) - 4 \log(8\beta^2) - \log(8\beta^2) \log\left(\frac{\mu^2}{m^2}\right) \right] \right\} \right). \end{aligned} \quad (2.7)$$

Here μ denotes the factorization and renormalization scales, which we keep equal in this analysis. The first line in both expressions contains the gluon corrections that can be attributed to the final-state particles, while the terms in the second line, proportional to either $C_F = (N_c^2 - 1)/(2N_c)$ or $C_A = N_c$ correspond to initial-state radiation from a quark or a gluon line, respectively. The final-state radiation consists of two parts. The logarithmic soft-emission terms are proportional to the colour charge of the final state [38, 25, 28, 30] and are therefore absent for the singlet colour state and proportional to C_A for the octet colour state. As a result, in the expression for the gluon-gluon fusion channel these terms are multiplied by $(N_c^2 - 4)/(N_c^2 - 2)$, which is the ratio of the colour-octet and the total cross section at threshold (cf. [38]). The Coulomb corrections receive contributions with colour factors C_F and the total colour charge of the final state. Note, finally, that the threshold behaviour of the cross section is determined by QCD dynamics and does not involve any supersymmetric parameters other than the mass of the produced stops.

2.1 Threshold resummation for the total inclusive cross section

In this paper we shall improve the NLO prediction for the hadroproduction of stop and sbottom pairs [3] by resumming the leading and next-to-leading threshold logarithms of the form

$$\alpha_s^n \log^m \beta^2 \quad , \quad m \leq 2n \quad (2.8)$$

¹Ref. [3] contains a misprint in the $\log(8\beta^2)$ -coefficient for the $q\bar{q}$ -channel. In Eq. (9) of [3] the coefficient $-107/(36\pi^2)$ should be replaced by $-155/(36\pi^2)$.

to all orders, and to next-to-leading logarithmic (NLL) accuracy. The resummation formalism developed for heavy-quark production [39, 38, 40] can be applied directly to squark-antisquark production as the colour structure is identical for both cases. The resummation is performed in the space of Mellin moments (N -space) following the procedure outlined in Refs. [25, 27, 30], where the hadroproduction of light-flavour squarks and gluinos at NLL accuracy has been considered.

From the viewpoint of threshold resummation there is a notable difference between the case of stops and light-flavour squarks, arising from the extra β^2 suppression of the quark-antiquark annihilation cross section $\sigma_{q\bar{q}\rightarrow t\bar{t}}$ near threshold. In N -space this effectively produces an extra factor $1/N$ compared to the light-flavour squark case, resulting in leading contributions $\propto \log^i(N)/N$ instead of $\log^i(N)$. For the seemingly analogous case of threshold resummation for the deep-inelastic structure function F_L , which has a leading behaviour of the type $\log^i(N)/N$ as well, differences from the expected NLL resummation structure were revealed in Refs. [41] and [42]. However, the NLL resummation procedure developed for light-flavour squarks applies to stop production as well. In the case of F_L the extra factor $1/N$ with respect to the N dependence of the structure function F_2 arises due to a special initial-state jet function [43, 44] associated with the longitudinal projection. In contrast, in our case the $\log^i(N)/N$ dependence arises from projecting onto the P -wave final state, which does not depend on the initial state jet function. Moreover, at $\mathcal{O}(\alpha_s)$ leading and subleading $\log(N)/N$ corrections can be computed from the one-loop calculations, and they do exhibit the pattern expected from NLL threshold resummation. Finally, in view of the different threshold behaviour of the $q\bar{q}$ and gg channels one might worry about the possibility that these channels mix in the NLL threshold resummation as a result of soft-quark emissions, which is not the case for top-quark and light-flavour squark production. However, we have checked that to NLL accuracy no such mixing occurs at $\mathcal{O}(\beta^3)$. Based on these observations we are confident that the expressions of Refs. [25, 27, 30] can be applied to inclusive stop-pair production as well.

The new elements that enter the NLL resummed cross section for stop pair production are the LO partonic cross sections in N -space (indicated by a tilde), decomposed into s -channel singlet and octet colour states. They are given by:

$$\tilde{\sigma}_{q\bar{q}\rightarrow t\bar{t},\mathbf{1}}^{(0)}(N) = 0, \quad (2.9)$$

$$\tilde{\sigma}_{q\bar{q}\rightarrow t\bar{t},\mathbf{8}}^{(0)}(N) = \frac{\alpha_s^2 \pi^{3/2}}{64m^2} \frac{N_c^2 - 1}{N_c^2} \frac{\Gamma(N+1)}{\Gamma(N+7/2)}, \quad (2.10)$$

$$\tilde{\sigma}_{gg\rightarrow t\bar{t},\mathbf{1}}^{(0)}(N) = \frac{\alpha_s^2 \pi^{3/2}}{16m^2} \frac{1}{N_c(N_c^2 - 1)} \frac{N(N+3) + 4}{(N+2)(N+3)} \frac{\Gamma(N+1)}{\Gamma(N+5/2)}, \quad (2.11)$$

$$\tilde{\sigma}_{gg\rightarrow t\bar{t},\mathbf{8}}^{(0)}(N) = \frac{N_c^2 - 4}{2} \sigma_{gg\rightarrow t\bar{t},\mathbf{1}}^{(0)}(N) + \frac{\alpha_s^2 \pi^{3/2}}{64m^2} \frac{N_c}{N_c^2 - 1} \frac{N(N+3) + 4}{(N+2)(N+3)} \frac{\Gamma(N+1)}{\Gamma(N+7/2)}. \quad (2.12)$$

The results for the gluon-gluon channels (2.11) and (2.12) agree with those presented in [27] for light-flavour squarks and $N_c = 3$, and are reproduced here for completeness for general $SU(N_c)$. Note that the results in [27] include an additional factor $2n_f$ from the summation over the L and R squarks of n_f light flavours.

2.2 Threshold resummation for the transverse-momentum distribution

Similar to the inclusive cross section, soft-gluon corrections can also dominate the transverse-momentum distribution of the stops if the production takes place sufficiently close to the edge of phase space. We now briefly review the general construction of threshold-resummed transverse-momentum distributions (cf. [31]-[37]) and its application to stop-pair production.

We start with the general framework applicable to the hadroproduction of a pair of massive coloured particles. Assuming that one of the final-state particles carries a transverse momentum p_T , the minimal energy necessary to produce the system is $2m_T$, where the transverse mass m_T is defined by

$$m_T = \sqrt{m^2 + p_T^2}. \quad (2.13)$$

For the p_T -distribution the dominant contributions originating from soft gluon emission have again the structure (2.8), with the variable β replaced by (cf. [45])

$$\beta_T = \sqrt{1 - 4m_T^2/s}. \quad (2.14)$$

Like in the case of the total inclusive cross section, the resummation of the logarithmic threshold corrections to p_T -distributions takes place in the space of Mellin moments. However, in this case the Mellin transform is taken with respect to the scaling variable $\hat{x}_T^2 = 4m_T^2/s$, i.e.

$$\frac{d\tilde{\sigma}_{ij \rightarrow kl}}{dp_T}(N, p_T, \mu^2) \equiv \int_0^1 d\hat{x}_T^2 (\hat{x}_T^2)^{N-1} \frac{d\sigma_{ij \rightarrow kl}}{dp_T}(\hat{x}_T^2, p_T, \mu^2) \quad (2.15)$$

for a generic partonic subprocess $ij \rightarrow kl$.

In N -moment space the resummed partonic p_T -distribution for the hadroproduction of two massive coloured particles is given by

$$\begin{aligned} \frac{d\tilde{\sigma}_{ij \rightarrow kl}^{(\text{res})}}{dp_T}(N, p_T, \mu^2) &= \sum_I \frac{d\tilde{\sigma}_{ij \rightarrow kl, I}^{(0)}}{dp_T}(N, p_T, \mu^2) C_{ij \rightarrow kl, I}(N, p_T, \mu^2) \\ &\times \Delta_i(N+1, Q^2, \mu^2) \Delta_j(N+1, Q^2, \mu^2) \Delta_{ij \rightarrow kl, I}^{(s)}(N+1, Q^2, \mu^2), \end{aligned} \quad (2.16)$$

with $Q = 2m_T$ representing the resummation scale and the index I indicating all possible colour states of the hard scattering. To NLL accuracy, the coefficients $C_{ij \rightarrow kl, I}(N, p_T, \mu^2)$ are equal to 1 for all channels and colour structures. The functions Δ_i and Δ_j sum the effects of the (soft-)collinear radiation from the incoming partons. They are process- and colour-independent, and are therefore a universal ingredient in all threshold-resummed cross sections. Explicit expressions for the Δ_i can for instance be found in Ref. [27]. The function $\Delta_{ij \rightarrow kl, I}^{(s)}$ accounts for soft wide-angle emission and depends on the production process and the colour channel. At NLL accuracy it is given by

$$\Delta_{ij \rightarrow kl, I}^{(s)}(N, Q^2, \mu^2) = \exp \left[\int_{\mu}^{Q/N} \frac{dq}{q} \frac{\alpha_s(q)}{\pi} D_{ij \rightarrow kl, I} \right]. \quad (2.17)$$

The values of the coefficients $D_{ij \rightarrow kl, I}$ follow from the threshold limit of the one-loop soft anomalous-dimension matrix in the way described e.g. in Ref. [30]. If an s -channel colour basis is used, the soft anomalous-dimension matrix for the p_T -distribution becomes diagonal in colour space in the threshold limit $\beta_T \rightarrow 0$, leading to the colour-diagonal form of the resummation formula given in Eq. (2.16). This is similar to threshold resummation for the total cross section, where the soft anomalous-dimension matrix becomes diagonal in colour space in the corresponding threshold limit $\beta \rightarrow 0$. Since the threshold limit is defined differently for the total inclusive cross section and the p_T -distribution, the values of the D -coefficients are different as well; in particular, the D -coefficients now carry p_T -dependence.

For the stop-pair production processes we have

$$D_{q\bar{q}/gg \rightarrow t\bar{t}, \mathbf{1}} = -2C_F (\text{Re } L_{\bar{\beta}_T} + 1) , \quad (2.18)$$

$$D_{q\bar{q}/gg \rightarrow t\bar{t}, \mathbf{8}} = -2C_F (\text{Re } L_{\bar{\beta}_T} + 1) + C_A \left[\log\left(\frac{m_T^2}{m^2}\right) + \text{Re } L_{\bar{\beta}_T} \right] , \quad (2.19)$$

with

$$\text{Re } L_{\bar{\beta}_T} = \frac{1 + \bar{\beta}_T^2}{2\bar{\beta}_T} \log\left(\frac{1 - \bar{\beta}_T}{1 + \bar{\beta}_T}\right) \quad (2.20)$$

and

$$\bar{\beta}_T = \lim_{\hat{x}_T^2 \rightarrow 1} \beta_T = \sqrt{1 - m^2/m_T^2} . \quad (2.21)$$

These expressions agree with those obtained for heavy-quark production in the context of joint resummation [37].

In addition to the soft radiative factor, the other new elements which have to be calculated in order to obtain resummed predictions from Eq. (2.16) are the colour-decomposed LO p_T -distributions in N -moment space. They are obtained from

$$\frac{d\sigma^{(0)}_{q\bar{q} \rightarrow t\bar{t}, \mathbf{1}}}{dp_T} = 0 , \quad (2.22)$$

$$\frac{d\sigma^{(0)}_{q\bar{q} \rightarrow t\bar{t}, \mathbf{8}}}{dp_T} = \frac{\alpha_s^2 \pi}{s^3} \frac{2(N_c^2 - 1)}{N_c^2} \frac{p_T^3}{\beta_T} , \quad (2.23)$$

$$\frac{d\sigma^{(0)}_{gg \rightarrow t\bar{t}, \mathbf{1}}}{dp_T} = \frac{\alpha_s^2 \pi}{s^2} \frac{2}{N_c(N_c^2 - 1)} \frac{p_T}{\beta_T} \frac{m^4 + p_T^4}{m_T^4} , \quad (2.24)$$

$$\frac{d\sigma^{(0)}_{gg \rightarrow t\bar{t}, \mathbf{8}}}{dp_T} = \frac{N_c^2 - 4}{2} \frac{d\sigma^{(0)}_{gg \rightarrow t\bar{t}, \mathbf{1}}}{dp_T} + \frac{\alpha_s^2 \pi}{s^2} \frac{N_c}{N_c^2 - 1} p_T \beta_T \frac{m^4 + p_T^4}{m_T^4} . \quad (2.25)$$

Taking a Mellin transform of (2.22)-(2.25) with respect to the threshold variable \hat{x}_T^2 one

finds

$$\frac{d\tilde{\sigma}_{q\bar{q}\rightarrow t\bar{t},\mathbf{1}}^{(0)}}{dp_T}(N) = 0, \quad (2.26)$$

$$\frac{d\tilde{\sigma}_{q\bar{q}\rightarrow t\bar{t},\mathbf{8}}^{(0)}}{dp_T}(N) = \frac{\alpha_s^2 \pi^{3/2}}{32} \frac{N_c^2 - 1}{N_c^2} \frac{\Gamma(N+3)}{\Gamma(N+7/2)} \frac{p_T^3}{m_T^6}, \quad (2.27)$$

$$\frac{d\tilde{\sigma}_{gg\rightarrow t\bar{t},\mathbf{1}}^{(0)}}{dp_T}(N) = \frac{\alpha_s^2 \pi^{3/2}}{8} \frac{1}{N_c(N_c^2 - 1)} \frac{\Gamma(N+2)}{\Gamma(N+5/2)} \frac{p_T(m^4 + p_T^4)}{m_T^8}, \quad (2.28)$$

$$\frac{d\tilde{\sigma}_{gg\rightarrow t\bar{t},\mathbf{8}}^{(0)}}{dp_T}(N) = \frac{N_c^2 - 4}{2} \frac{d\tilde{\sigma}_{gg\rightarrow t\bar{t},\mathbf{1}}^{(0)}}{dp_T}(N) + \frac{\alpha_s^2 \pi^{3/2}}{32} \frac{N_c}{N_c^2 - 1} \frac{\Gamma(N+2)}{\Gamma(N+7/2)} \frac{p_T(m^4 + p_T^4)}{m_T^8}. \quad (2.29)$$

Having calculated the resummed partonic expression in N -space, Eq. (2.16), the resummed hadronic p_T -distribution is obtained by the inverse Mellin transform

$$\begin{aligned} \frac{d\sigma_{h_1 h_2 \rightarrow kl}^{(\text{res})}}{dp_T}(x_T^2, p_T, \mu^2) &= \sum_{i,j=q,\bar{q},g} \int_{\text{CT}} \frac{dN}{2\pi i} (x_T^2)^{-N} \tilde{f}_{i/h_1}(N+1, \mu^2) \tilde{f}_{j/h_2}(N+1, \mu^2) \\ &\quad \times \frac{d\tilde{\sigma}_{ij\rightarrow kl}^{(\text{res})}}{dp_T}(N, p_T, \mu^2), \end{aligned} \quad (2.30)$$

where $x_T^2 = 4m_T^2/S$ is the hadronic scaling variable. The functions \tilde{f}_{i/h_1} and \tilde{f}_{j/h_2} are the Mellin moments of the parton distribution functions for the initial-state hadrons h_1 and h_2 . In order to retain the information contained in the NLO p_T -distributions [3], the NLO and NLL results are combined through a matching procedure that avoids double counting of the logarithmic terms in the following way:

$$\begin{aligned} \frac{d\sigma_{h_1 h_2 \rightarrow kl}^{(\text{NLO+NLL})}}{dp_T}(x_T^2, p_T, \mu^2) &= \frac{d\sigma_{h_1 h_2 \rightarrow kl}^{(\text{NLO})}}{dp_T}(x_T^2, p_T, \mu^2) \\ &\quad + \sum_{i,j=q,\bar{q},g} \int_{\text{CT}} \frac{dN}{2\pi i} (x_T^2)^{-N} \tilde{f}_{i/h_1}(N+1, \mu^2) \tilde{f}_{j/h_2}(N+1, \mu^2) \\ &\quad \times \left[\frac{d\tilde{\sigma}_{ij\rightarrow kl}^{(\text{res})}}{dp_T}(N, p_T, \mu^2) - \frac{d\tilde{\sigma}_{ij\rightarrow kl}^{(\text{res})}}{dp_T}(N, p_T, \mu^2) \Big|_{(\text{NLO})} \right], \end{aligned} \quad (2.31)$$

where $(d\tilde{\sigma}^{(\text{res})}/dp_T)|_{(\text{NLO})}$ represents the perturbative expansion of the NLL p_T -distribution (2.16) truncated at the order of α_s associated with NLO. To evaluate the inverse Mellin transform in Eqs. (2.30) and (2.31) we adopt the ‘‘minimal prescription’’ of Ref. [46] for the integration contour CT.

3. Numerical results

We present numerical results for the NLL-resummed cross sections and transverse-momentum distributions matched with the complete NLO results for stop-pair production at the

Tevatron ($\sqrt{S} = 1.96$ TeV) and the LHC ($\sqrt{S} = 7$ and 14 TeV). The matching procedures for the total cross section and for the transverse-momentum distribution are described in Ref. [30] and in Eq. (2.31), respectively. We use the notation NLO+NLL for matched quantities in the following. The NLO corrections are calculated using `Prospino` [23], based on the calculation presented in Ref. [3]. The QCD coupling α_s and the parton distribution functions (pdfs) at NLO are defined in the $\overline{\text{MS}}$ scheme with five active flavours. The mass of the stop is renormalized in the on-shell scheme and the SUSY particles are decoupled from the running of α_s and the pdfs. Since mixing enters explicitly only through higher-order diagrams, the angle $\theta_{\tilde{t}}$ need not be renormalized and one can use the lowest-order expression derived from the stop mass matrix.

As our default, hadronic total cross sections and transverse-momentum distributions are obtained with the 2008 NLO MSTW pdfs [47] and the corresponding $\alpha_s(M_Z) = 0.120$. The NLL corrections are convoluted with pdfs in Mellin space, derived with the program `PEGASUS` [49] based on the MSTW parametrization at the initial factorization scale. For the total hadronic cross sections, we have also used the method of Ref. [50] to evaluate the NLL cross section with standard parametrizations of pdfs in x -space. We find however a much better numerical stability when the total NLL cross sections are evaluated with Mellin-space pdfs.

Beyond LO the cross section does not only depend on the stop mass, but also on the gluino mass $m_{\tilde{g}}$, the average mass of the first and second generation squarks $m_{\tilde{q}}$ and the mixing angle $\theta_{\tilde{t}}$. For this reason we have adopted the SPS1a' benchmark scenario [51] for our numerical analysis. Taking a top-quark mass of $m_t = 172.5$ GeV [52] and $\alpha_s(M_Z) = 0.120$ the SPS1a' scenario corresponds to $m_{\tilde{g}} = 610$ GeV, $m_{\tilde{q}} = 560$ GeV, $\sin(2\theta_{\tilde{t}}) = 0.932$ and stop masses of $m_{\tilde{t}_1} = 367$ GeV and $m_{\tilde{t}_2} = 590$ GeV [53]. However, in order to focus on the mass dependence of the cross section and the NLO+NLL corrections, we vary the mass of the stop while keeping the other SUSY parameters fixed. As shown in Ref. [3] and discussed in more detail in the appendix, the dependence of the cross section on the additional SUSY parameters is small, justifying this procedure. Note that the numerical results presented for stop production also apply to sbottom production when the same input parameters are adopted. In the appendix we show that the impact of bottom-quark induced contributions to sbottom hadroproduction is negligible and present benchmark predictions for the sbottom cross section.

3.1 Results for the total cross section

Let us first discuss the scale dependence of the SUSY-QCD total cross-section prediction. Fig. 2 shows the scale dependence in LO, NLO and NLO+NLL for $\tilde{t}_1 \bar{\tilde{t}}_1$ production, using $m_{\tilde{t}_1} = 200$ GeV and 500 GeV at the Tevatron and LHC, respectively. Here and in the following, we present results for the LHC operating at 7 TeV and at 14 TeV centre-of-mass energy. Note that the LO predictions are obtained with LO pdfs and the corresponding LO values for α_s [47]. The renormalization and factorization scales are identified and varied around the central scale $\mu_0 = m_{\tilde{t}_1}$ from $\mu = \mu_0/10$ up to $\mu = 5\mu_0$. We observe the usual strong reduction of the scale dependence when going from LO to NLO. A further significant

improvement is obtained when the resummation of threshold logarithms is included, in particular for stop production at the Tevatron and at the LHC running at 7 TeV.

Near the central scale $\mu = m_{\tilde{t}_1}$ the cross section is enhanced by the SUSY-QCD corrections at NLO and NLO+NLL. The size of the K -factors $K_{\text{NLO}} \equiv \sigma_{\text{NLO}}/\sigma_{\text{LO}}$ and $K_{\text{NLL}} \equiv \sigma_{\text{NLO+NLL}}/\sigma_{\text{NLO}}$ strongly depends on the stop mass and the collider, as is shown in Fig. 3. At the Tevatron, where the cross section is dominated by $q\bar{q}$ -annihilation for large stop masses, the NLO K -factor is moderate and ranges from roughly 1.2 to 1.03 for stop masses in the range between 100 and 300 GeV. A further enhancement by up to 7% is found for large stop masses when the NLL resummation is included. At the LHC, the gg initial state is dominant and the QCD corrections are in general larger. For $\tilde{t}_1\bar{\tilde{t}}_1$ and $\tilde{t}_2\bar{\tilde{t}}_2$ production at the LHC we consider the mass ranges $100 \text{ GeV} \leq m_{\tilde{t}_1} \leq 550 \text{ GeV}$ (lower horizontal axis) and $550 \text{ GeV} \leq m_{\tilde{t}_2} \leq 1 \text{ TeV}$ (upper horizontal axis). At 7 TeV we find NLO corrections ranging from about 40% at the lower end of the stop mass range to about 20% for stop masses near 1 TeV. The NLL resummation leads to a further increase of the cross-section prediction of approximately 10% for stop masses in the TeV-range. At 14 TeV centre-of-mass energy the NLO corrections to stop production are significant and increase the LO cross section by around 35% for moderate \tilde{t}_1 masses and by up to 40% for \tilde{t}_2 with $m_{\tilde{t}_2} \approx 600 \text{ GeV}$, while the impact of the NLL resummation is modest with at most 5% further increase for stop masses in the TeV-range. The singularities at the stop-decay threshold $m_{\tilde{t}} = m_t + m_{\tilde{g}} = 782.5 \text{ GeV}$ originate from the stop wave-function renormalization. They are an unphysical artefact of the on-shell approach of Ref. [3] and could be removed by taking into account the finite widths of the unstable stops. Note that the NLO cross sections for $\tilde{t}_1\bar{\tilde{t}}_1$ and $\tilde{t}_2\bar{\tilde{t}}_2$ production are not identical, even if the masses are taken equal. The reason for this is that the stop mixing angle contributes in different ways to both reactions at NLO, as discussed in section 2. Furthermore, while we vary the mass of the stop particle that appears in the final state, the mass of the other stop, which enters the loop corrections, is set to its SPS1a' value and thus differs for \tilde{t}_1 and \tilde{t}_2 . However, numerically the difference between the two NLO total cross sections is moderate. The NLL resummation does not involve any SUSY parameters apart from the stop mass itself and thus affects the $\tilde{t}_1\bar{\tilde{t}}_1$ and $\tilde{t}_2\bar{\tilde{t}}_2$ cross sections in the same way. The NLL K -factors have a tiny SUSY-parameter dependence, which enters through the ratio $\sigma_{\text{NLO+NLL}}/\sigma_{\text{NLO}}$.

Predictions for the LO, NLO, and NLO+NLL total cross sections are shown in Fig. 4 and Tables 1–3 for $\tilde{t}_1\bar{\tilde{t}}_1$ production at the Tevatron and $\tilde{t}_1\bar{\tilde{t}}_1/\tilde{t}_2\bar{\tilde{t}}_2$ production at the LHC with 7 TeV and 14 TeV centre-of-mass energy. In fact, the cross sections for $\tilde{t}_1\bar{\tilde{t}}_1$ and $\tilde{t}_2\bar{\tilde{t}}_2$ production at equal masses are indistinguishable on the scale of Fig. 4. We thus refrain from showing additional plots for $\tilde{t}_2\bar{\tilde{t}}_2$ production. The results shown in Fig. 4 represent the state-of-the-art SUSY-QCD predictions at NLO+NLL accuracy. The error bands include the NLO+NLL scale variation in the range $m_{\tilde{t}_1}/2 \leq \mu \leq 2m_{\tilde{t}_1}$ as well as the NLO pdf uncertainty, added in quadrature. The pdf uncertainty is obtained with the help of the 90% C.L. MSTW error pdfs [48]. More detailed information is available in Tables 1–3.

In Table 1 we present results for $\tilde{t}_1\bar{\tilde{t}}_1$ production at the Tevatron. As discussed before, we observe an increase of the cross-section prediction near the central scale when going from LO to NLO and a further enhancement when NLL threshold resummation is included. The

scale dependence in the range $m_{\tilde{t}_1}/2 \leq \mu \leq 2m_{\tilde{t}_1}$ is reduced from about $\pm 50\%$ at LO to about $\pm 10\%$ at NLO+NLL. The estimated pdf uncertainty is approximately 5%. We also present cross-section predictions obtained with the CTEQ6 pdf set [54] and an estimate of the corresponding pdf error. The difference between the MSTW and CTEQ results is particularly pronounced at large stop masses, $m_{\tilde{t}_1} \approx 300$ GeV, where the cross sections obtained with CTEQ pdfs are about 7% larger than the ones obtained with MSTW pdfs. We observe that the CTEQ pdf error estimate of about 10% is roughly twice as large as that of MSTW.

Results for $\tilde{t}_1\tilde{t}_1$ and $\tilde{t}_2\tilde{t}_2$ production at the LHC with 7 TeV are collected in Table 2. Here the impact of the SUSY-QCD corrections at NLO is large, with the NLL resummation adding a further enhancement of up to 10%. The scale uncertainty of the NLO+NLL prediction is reduced to a level of about 10%. Unfortunately the pdf error is sizeable, in particular at stop masses in the TeV-region, where we find a pdf error of about 20% from MSTW. Also the difference between MSTW and CTEQ is significant for large stop masses, with a 25% increase in the prediction for stop masses near 1 TeV when going from MSTW to CTEQ pdfs. As before, we find a pdf error from the CTEQ analysis that is about twice as large as that of MSTW and reaches 45% for $m_{\tilde{t}_i} \approx 1$ TeV. Of course, the large pdf uncertainty is not a specific feature of stop production. It rather generically affects predictions for TeV-scale particle production at the LHC with 7 TeV centre-of-mass energy, since these predictions are particularly sensitive to the gluon pdf at large x (see e.g. Ref. [55]). The conclusion therefore is that more accurate pdf determinations are needed in order to allow for a precise prediction of heavy-particle production during the initial phase of the LHC at 7 TeV centre-of-mass energy.

Going from 7 TeV to 14 TeV at the LHC, we observe in Table 3 a significant increase in the predicted cross section of about a factor of 4 for stop masses around 100 GeV and up to a factor of about 60 for masses in the TeV-region and MSTW pdfs. Just like at 7 TeV, the scale uncertainty of the NLO+NLL prediction is down to a level of about 10%. The pdf uncertainty is more moderate than at 7 TeV, ranging from 3% at small masses to about 10% at large stop masses for MSTW, and correspondingly from 3% to 20% for CTEQ.

3.2 Results for the transverse-momentum distribution

Let us now turn to the discussion of the transverse-momentum distributions. Figure 5 shows a comparison between the LO, NLO and NLO+NLL distributions normalized to unity. We use normalized distributions in order to be able to directly read off the NLO- and NLL-induced changes in the shape of the distribution. As for the previous results, we have used the stop mass as the central scale, $\mu = m$, in Figure 5. This is a possible choice as we do not consider regions where $p_T \gg m$ and where a p_T -dependent scale would have been mandatory. As already observed in Ref. [56], the transverse momentum carried away by hard gluon radiation in higher orders softens the NLO transverse-momentum distribution with respect to the LO distribution. This effect is particularly visible at the Tevatron and at the LHC with 7 TeV centre-of-mass energy. The NLL soft-gluon resummation, on the other hand, does not affect the shape of the distribution significantly. To elucidate the

impact of the higher-order corrections more clearly, we display the transverse-momentum dependence of the NLO and NLL K -factors in Figure 6, this time using the transverse mass $m_T = \sqrt{m^2 + p_T^2}$ as the scale. The significant softening of the transverse-momentum distribution at NLO at the Tevatron and the 7 TeV LHC is reflected in the variation of the K -factor, with K_{NLO} dropping from roughly 1.8 at small p_T to a value near one at $p_T \approx 2m$. In comparison, the impact of the NLL resummation is small. A similar behaviour, albeit less pronounced, is observed at the LHC with 14 TeV centre-of-mass energy. It would be interesting to see if using NLO+NLL transverse-momentum distributions would affect the experimental analyses, which so far have been based on LO Monte Carlo predictions. In this context we recall that the shape of the stop rapidity distribution is not changed significantly by higher-order corrections, see Ref. [56].

4. Conclusions

In this paper we have performed the NLL threshold resummation for stop and sbottom hadroproduction, considering both the inclusive cross sections and the transverse-momentum distributions. As the lighter stop and sbottom mass eigenstates are generally predicted to be the lightest strongly interacting SUSY particles, the search for these particles plays a special role in the quest to find signals of supersymmetry at hadron colliders.

Results have been given for the Tevatron and for the LHC running at both 7 TeV and 14 TeV centre-of-mass energy. Compared to the NLO predictions for the total cross section, the NLL corrections lead to a significant reduction of the scale dependence and increase the cross section by up to 10% for masses in the TeV range if the renormalization and factorization scales are chosen close to the mass of the final-state particles. We have also studied the SUSY parameter dependence of the stop and sbottom cross sections and find small variations of at most 2%. The size of bottom-induced contributions to sbottom pair production is negligible numerically so that predictions obtained for stop-pair production also apply to sbottom-pair production when the same input parameters are adopted.

Since p_T cuts are used extensively in experimental analyses, which at present are based on LO Monte Carlo simulations, it is important to investigate how the NLO+NLL matched corrections affect the transverse-momentum distributions. We find that the NLO+NLL corrections can change the shape of the p_T distribution considerably and thus generally cannot be taken into account by using a simple K -factor.

The NLO+NLL matched cross sections and p_T distributions presented in this paper constitute the state-of-the-art QCD predictions for stop and sbottom production and can be employed to improve current and future searches at the Tevatron and LHC.

Acknowledgments

We would like to thank Sven Moch, James Stirling, Robert Thorne and Andreas Vogt for valuable discussions and the MSTW collaboration for providing us with parton distribution functions with improved accuracy in the evolution at large x . This work has been supported in part by the Helmholtz Alliance “Physics at the Terascale”, the DFG Graduiertenkolleg “Elementary Particle Physics at the TeV Scale”, the Foundation for Fundamental Research of Matter (FOM), the National Organization for Scientific Research (NWO), the DFG SFB/TR9 “Computational Particle Physics”, and the European Community’s Marie-Curie Research Training Network under contract MRTN-CT-2006-035505 “Tools and Precision Calculations for Physics Discoveries at Colliders”. SB would like to thank the Nikhef Theory Group, and MK would like to thank the Institute for High Energy Physics (IFAE) at the Universitat Aut3noma de Barcelona and the CERN TH unit for their hospitality. AK acknowledges the hospitality of the Institute of Theoretical Physics at the University of Warsaw.

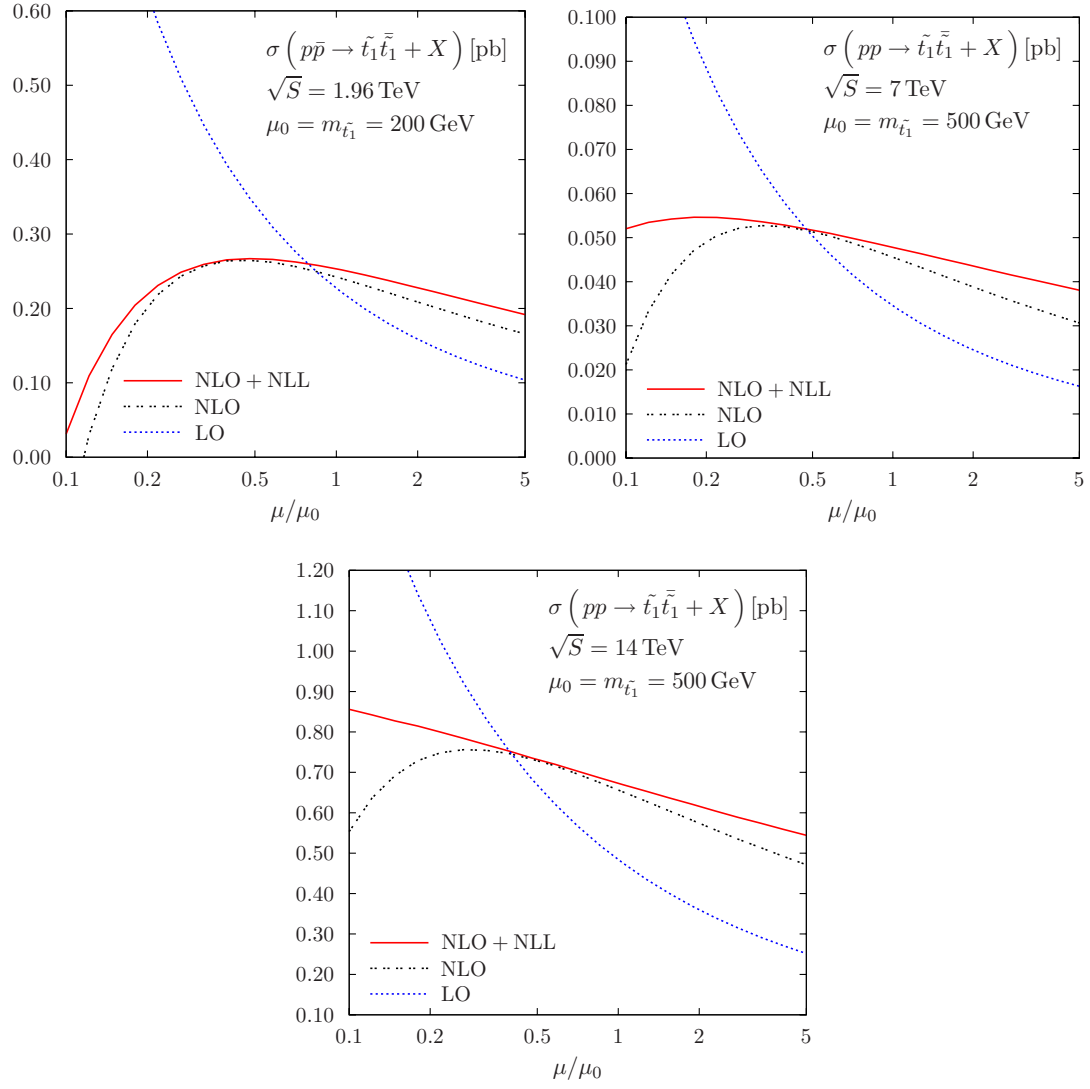


Figure 2: Scale dependence of the LO, NLO and NLO+NLL cross section for stop-antistop production at the Tevatron and the LHC.

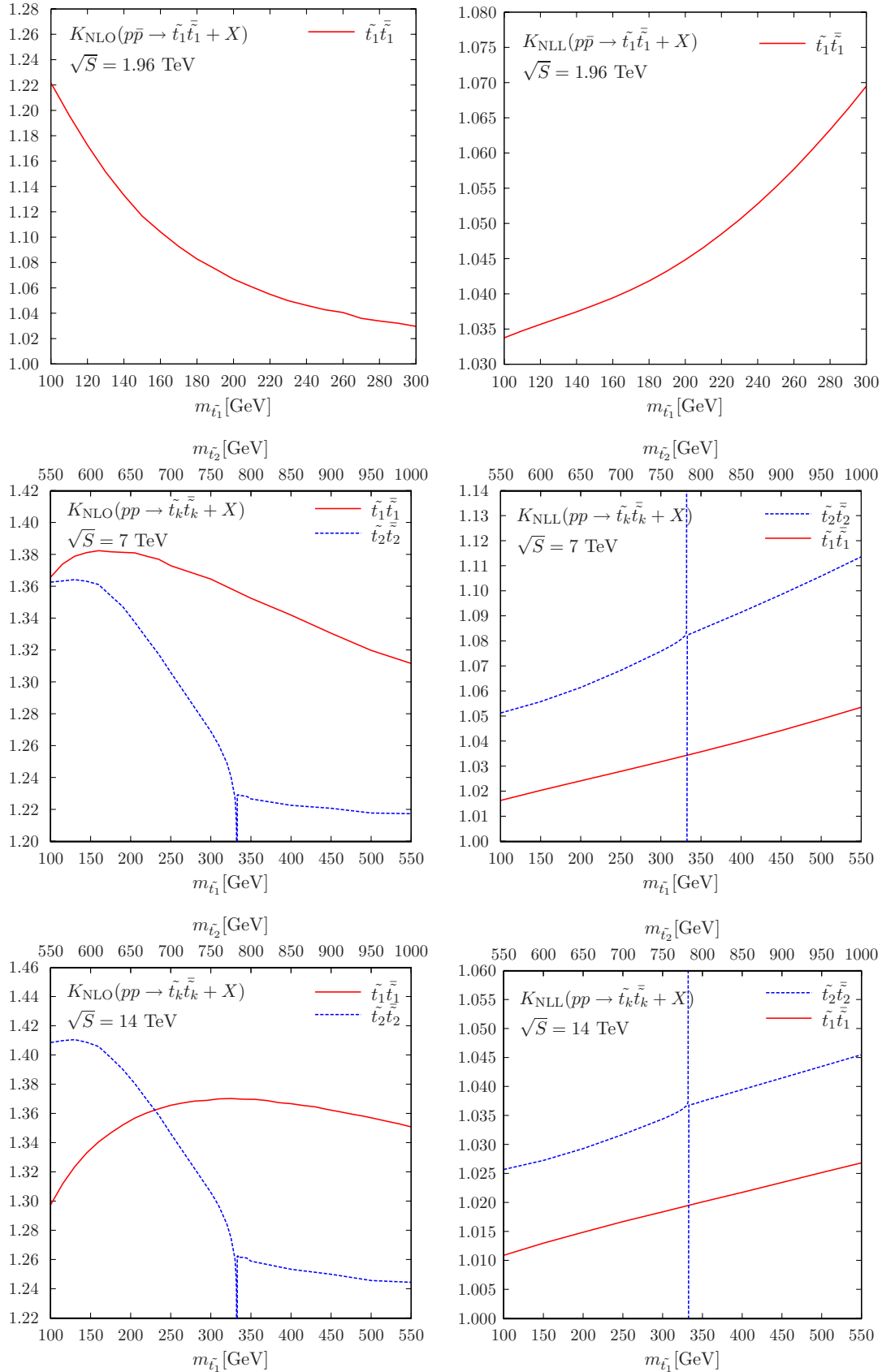


Figure 3: The NLO and NLL K -factors for stop-antistop production at the Tevatron and the LHC as a function of the stop mass. The scale has been set to the stop mass, i.e. $\mu = m_{\tilde{t}_k}$.

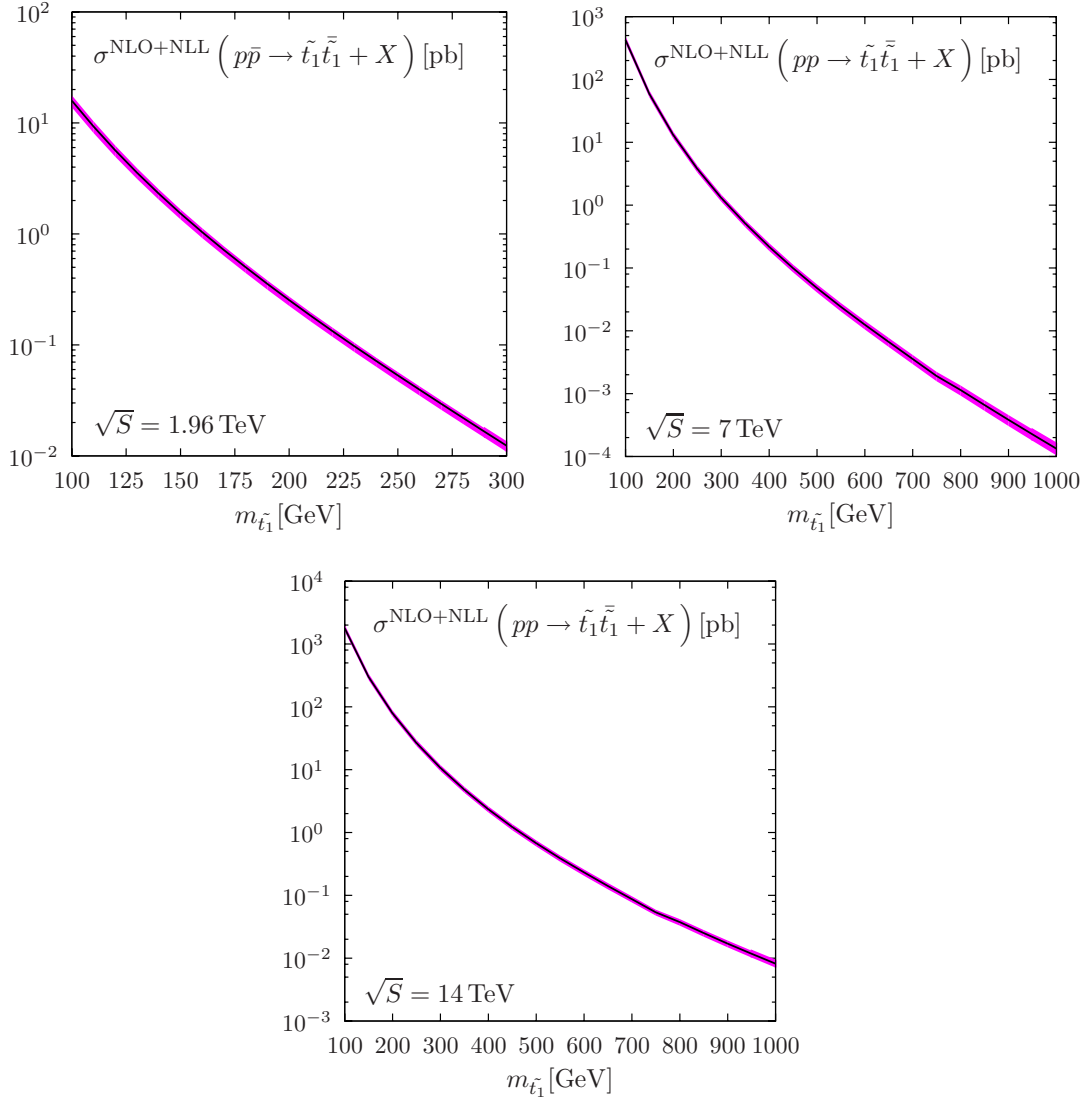


Figure 4: Total NLO+NLL stop-pair cross section at the Tevatron and the LHC as a function of the stop mass. The error band corresponds to the scale and pdf uncertainty of the prediction, added in quadrature.

$p\bar{p} \rightarrow \tilde{t}_1 \bar{\tilde{t}}_1$ at $\sqrt{S} = 1.96$ TeV

$m_{\tilde{t}_1}$ [GeV]	MSTW2008			CTEQ6.6M		
	100	200	300	100	200	300
$(\sigma \pm \Delta\sigma_\mu)_{\text{LO}}$ [pb]	$12.6^{+6.4}_{-3.9}$	$0.227^{+0.112}_{-0.068}$	$(1.12^{+0.57}_{-0.35}) \times 10^{-2}$	$10.3^{+4.3}_{-2.9}$	$0.210^{+0.091}_{-0.059}$	$(1.20^{+0.51}_{-0.33}) \times 10^{-2}$
$(\sigma \pm \Delta\sigma_\mu)_{\text{NLO}}$ [pb]	$15.3^{+2.0}_{-2.4}$	$0.242^{+0.022}_{-0.034}$	$(1.15^{+0.12}_{-0.17}) \times 10^{-2}$	$14.7^{+1.8}_{-2.2}$	$0.249^{+0.022}_{-0.034}$	$(1.23^{+0.13}_{-0.18}) \times 10^{-2}$
$(\sigma \pm \Delta\sigma_\mu)_{\text{NLO+NLL}}$ [pb]	$15.9^{+1.6}_{-1.8}$	$0.253^{+0.014}_{-0.025}$	$(1.24^{+0.07}_{-0.13}) \times 10^{-2}$	$15.1^{+1.4}_{-1.6}$	$0.260^{+0.014}_{-0.025}$	$(1.31^{+0.08}_{-0.14}) \times 10^{-2}$
$\Delta\text{pdf}_{\text{NLO}}$ [%]	± 6.6	± 5.3	± 5.3	± 11	± 11	± 11
K_{NLO}	1.22	1.07	1.03	1.43	1.19	1.10
K_{NLL}	1.03	1.05	1.07	1.03	1.04	1.07

Table 1: The LO, NLO and NLO+NLL cross sections for stop-antistop production at the Tevatron ($\sqrt{S}=1.96$ TeV), including errors due to scale variation ($\Delta\sigma_\mu$) in the range $m_{\tilde{t}_1}/2 \leq \mu \leq 2m_{\tilde{t}_1}$. Results are shown for two pdf parametrizations (MSTW08 and CTEQ6) with the corresponding 90% C.L. pdf error estimates.

$$pp \rightarrow \tilde{t}_1 \bar{\tilde{t}}_1 \text{ at } \sqrt{S} = 7 \text{ TeV}$$

MSTW2008			CTEQ6.6M	
$m_{\tilde{t}_1}$ [GeV]	100	400	100	400
$(\sigma \pm \Delta\sigma_\mu)_{\text{LO}}$ [pb]	305^{+114}_{-77}	$0.156^{+0.070}_{-0.044}$	265^{+95}_{-65}	$0.119^{+0.048}_{-0.032}$
$(\sigma \pm \Delta\sigma_\mu)_{\text{NLO}}$ [pb]	416^{+64}_{-59}	$0.209^{+0.027}_{-0.031}$	384^{+57}_{-52}	$0.202^{+0.025}_{-0.028}$
$(\sigma \pm \Delta\sigma_\mu)_{\text{NLO+NLL}}$ [pb]	423^{+60}_{-46}	$0.218^{+0.020}_{-0.020}$	390^{+53}_{-41}	$0.209^{+0.018}_{-0.019}$
$\Delta\text{pdf}_{\text{NLO}}$ [%]	± 3.9	± 10	± 3.4	± 17
K_{NLO}	1.37	1.34	1.45	1.70
K_{NLL}	1.02	1.04	1.02	1.04

$$pp \rightarrow \tilde{t}_2 \bar{\tilde{t}}_2 \text{ at } \sqrt{S} = 7 \text{ TeV}$$

MSTW2008			CTEQ6.6M	
$m_{\tilde{t}_2}$ [GeV]	600	1000	600	1000
$(\sigma \pm \Delta\sigma_\mu)_{\text{LO}}$ [pb]	$(9.06^{+4.22}_{-2.66}) \times 10^{-3}$	$(9.64^{+4.83}_{-2.97}) \times 10^{-5}$	$(6.63^{+2.70}_{-1.78}) \times 10^{-3}$	$(6.76^{+2.86}_{-1.88}) \times 10^{-5}$
$(\sigma \pm \Delta\sigma_\mu)_{\text{NLO}}$ [pb]	$(1.23^{+0.18}_{-0.20}) \times 10^{-2}$	$(1.17^{+0.18}_{-0.20}) \times 10^{-4}$	$(1.27^{+0.18}_{-0.20}) \times 10^{-2}$	$(1.50^{+0.18}_{-0.24}) \times 10^{-4}$
$(\sigma \pm \Delta\sigma_\mu)_{\text{NLO+NLL}}$ [pb]	$(1.30^{+0.13}_{-0.12}) \times 10^{-2}$	$(1.31^{+0.05}_{-0.09}) \times 10^{-4}$	$(1.33^{+0.13}_{-0.13}) \times 10^{-2}$	$(1.64^{+0.07}_{-0.11}) \times 10^{-4}$
$\Delta\text{pdf}_{\text{NLO}}$ [%]	± 15	± 23	± 26	± 46
K_{NLO}	1.36	1.22	1.92	2.21
K_{NLL}	1.06	1.11	1.05	1.10

Table 2: The LO, NLO and NLO+NLL cross sections for stop-antistop production at the LHC ($\sqrt{S}=7$ TeV), including errors due to scale variation ($\Delta\sigma_\mu$) in the range $m_{\tilde{t}}/2 \leq \mu \leq 2m_{\tilde{t}}$. Results are shown for two pdf parametrizations (MSTW08 and CTEQ6) with the corresponding 90% C.L. pdf error estimates.

$pp \rightarrow \tilde{t}_1 \bar{\tilde{t}}_1$ at $\sqrt{S} = 14$ TeV

MSTW2008			CTEQ6.6M	
$m_{\tilde{t}_1}$ [GeV]	100	400	100	400
$(\sigma \pm \Delta\sigma_\mu)_{\text{LO}}$ [pb]	$(1.35^{+0.41}_{-0.29}) \times 10^3$	$1.67^{+0.62}_{-0.42}$	$(1.22^{+0.35}_{-0.26}) \times 10^3$	$1.40^{+0.49}_{-0.34}$
$(\sigma \pm \Delta\sigma_\mu)_{\text{NLO}}$ [pb]	$(1.75^{+0.26}_{-0.22}) \times 10^3$	$2.29^{+0.25}_{-0.29}$	$(1.63^{+0.23}_{-0.19}) \times 10^3$	$2.14^{+0.24}_{-0.26}$
$(\sigma \pm \Delta\sigma_\mu)_{\text{NLO+NLL}}$ [pb]	$(1.77^{+0.24}_{-0.17}) \times 10^3$	$2.34^{+0.21}_{-0.21}$	$(1.65^{+0.22}_{-0.16}) \times 10^3$	$2.19^{+0.20}_{-0.19}$
$\Delta\text{pdf}_{\text{NLO}}$ [%]	± 2.8	± 6.2	± 2.6	± 8.6
K_{NLO}	1.30	1.37	1.34	1.53
K_{NLL}	1.01	1.02	1.01	1.02

$pp \rightarrow \tilde{t}_2 \bar{\tilde{t}}_2$ at $\sqrt{S} = 14$ TeV

MSTW2008			CTEQ6.6M	
$m_{\tilde{t}_2}$ [GeV]	600	1000	600	1000
$(\sigma \pm \Delta\sigma_\mu)_{\text{LO}}$ [pb]	$0.167^{+0.065}_{-0.043}$	$(6.13^{+2.51}_{-1.65}) \times 10^{-3}$	$0.135^{+0.048}_{-0.033}$	$(4.71^{+1.72}_{-1.17}) \times 10^{-3}$
$(\sigma \pm \Delta\sigma_\mu)_{\text{NLO}}$ [pb]	$0.235^{+0.030}_{-0.031}$	$(7.63^{+0.65}_{-0.92}) \times 10^{-3}$	$0.225^{+0.027}_{-0.029}$	$(7.65^{+0.62}_{-0.90}) \times 10^{-3}$
$(\sigma \pm \Delta\sigma_\mu)_{\text{NLO+NLL}}$ [pb]	$0.242^{+0.024}_{-0.022}$	$(7.98^{+0.36}_{-0.51}) \times 10^{-3}$	$0.230^{+0.022}_{-0.020}$	$(7.97^{+0.35}_{-0.50}) \times 10^{-3}$
$\Delta\text{pdf}_{\text{NLO}}$ [%]	± 8.3	± 12	± 13	± 21
K_{NLO}	1.41	1.24	1.66	1.62
K_{NLL}	1.03	1.05	1.03	1.04

Table 3: The LO, NLO and NLO+NLL cross sections for stop-antistop production at the LHC ($\sqrt{S}=14$ TeV), including errors due to scale variation ($\Delta\sigma_\mu$) in the range $m_{\tilde{t}}/2 \leq \mu \leq 2m_{\tilde{t}}$. Results are shown for two pdf parametrizations (MSTW08 and CTEQ6) with the corresponding 90% C.L. pdf error estimates.

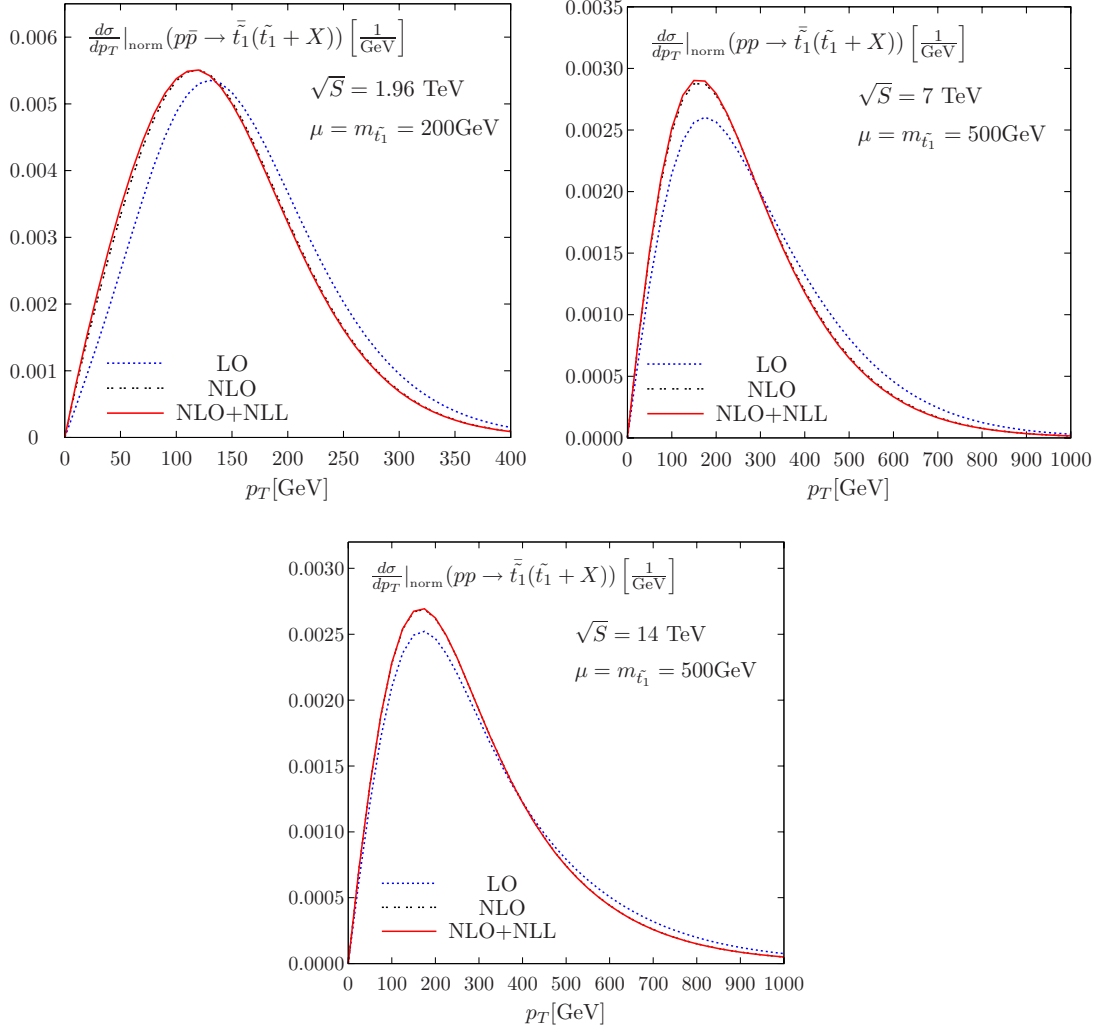


Figure 5: Normalized LO, NLO and NLO+NLL transverse-momentum distributions for stop-antistop production at the Tevatron and the LHC for $\mu = m_{\tilde{t}_1}$.

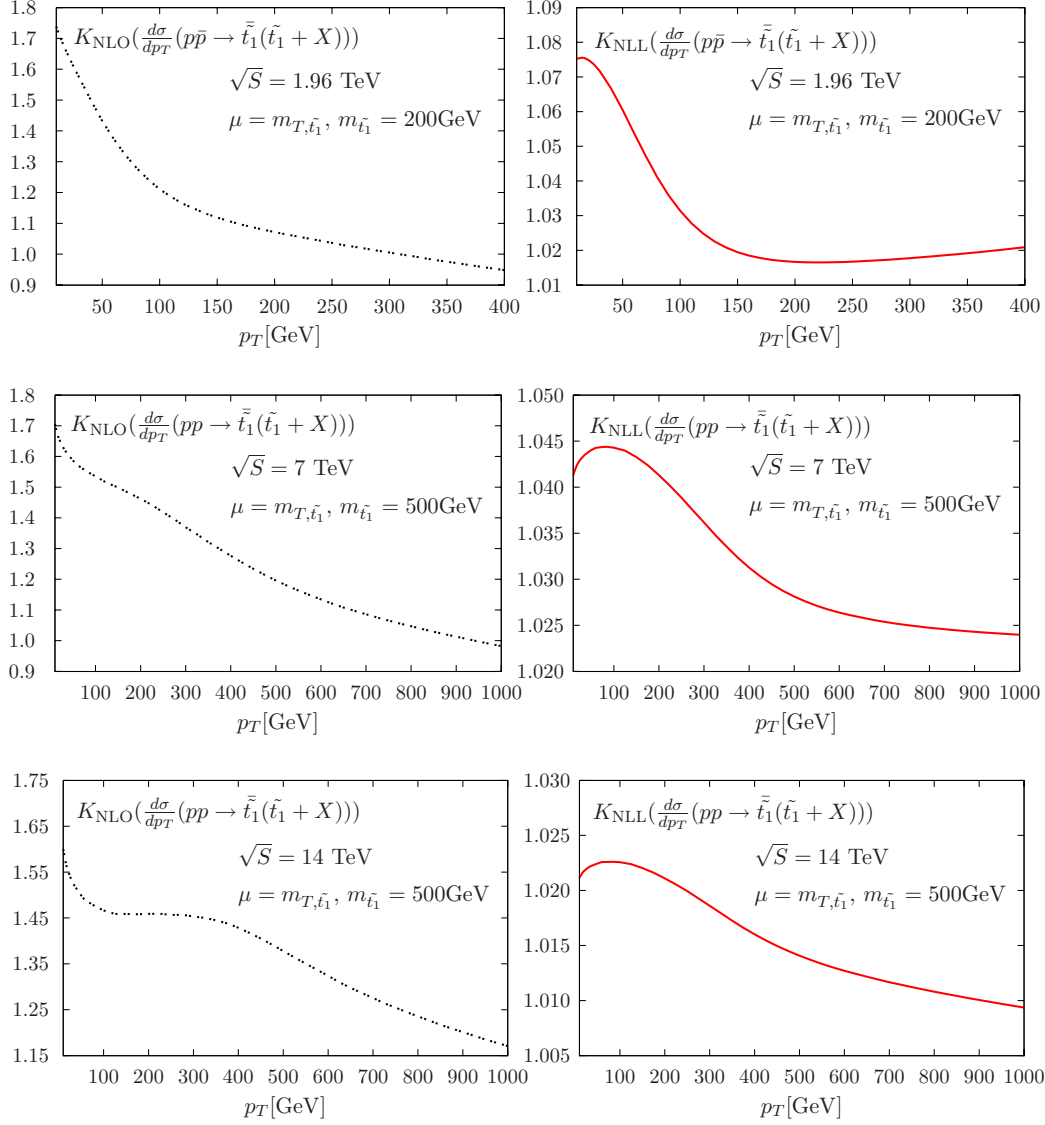


Figure 6: Transverse-momentum dependence of the NLO and NLL K -factors for stop-antistop production at the Tevatron and the LHC for $\mu = m_{T, \tilde{t}_1}$.

A. SUSY parameter dependence of stop and sbottom cross sections

In this appendix we shall investigate the dependence of the NLO+NLL stop and sbottom cross-section predictions on the supersymmetric model parameters that enter beyond LO, i.e. the mixing angle and the masses of the light-flavour squarks and the gluino. In the case of sbottom production we shall in addition quantify the impact of the bottom-quark-induced reaction channels $b\bar{b} \rightarrow \tilde{b}_k\bar{\tilde{b}}_k$ and $bb/\bar{b}\bar{b} \rightarrow \tilde{b}_k\bar{\tilde{b}}_k/\bar{\tilde{b}}_k\tilde{b}_k$, involving contributions from t -channel gluino exchange. It will be demonstrated that the contributions of these partonic reaction channels are strongly suppressed numerically. Thus, for all practical purposes, cross-section predictions obtained for stop-pair production also apply to sbottom-pair production when the same input parameters are adopted.

As in the main body of the paper we choose the SPS1a' benchmark scenario [51] as our default. The SPS1a' masses and mixings relevant for stop and sbottom hadroproduction are collected in Table 4. Note that the stop and sbottom masses predicted by the SPS1a' and

SPS1a'					
$m_{\tilde{t}_1}$	367 GeV	$m_{\tilde{b}_1}$	509 GeV	$m_{\tilde{g}}$	560 GeV
$m_{\tilde{t}_2}$	590 GeV	$m_{\tilde{b}_2}$	549 GeV	$m_{\tilde{g}}$	610 GeV
$\sin 2\theta_{\tilde{t}}$	0.932	$\sin 2\theta_{\tilde{b}}$	0.652		

Table 4: Masses and mixings for the SPS1a' benchmark scenario [51] obtained using SPheno [53] with the Standard Model input parameters $m_t = 172.5$ GeV and $\alpha_s(M_Z) = 0.120$.

other commonly used benchmark scenarios are beyond the reach of the Tevatron searches, as the corresponding production cross sections are too small. The SPS1a' NLO+NLL cross sections for stop and sbottom production at the LHC are collected in Table 5.

From the cross-section predictions one can conclude that only the lighter of the SPS1a' stop mass eigenstates might be detected during the initial phase of LHC data taking at 7 TeV with 1 fb^{-1} of integrated luminosity. Also a dedicated search for sbottom production in SPS1a'-like scenarios will only be possible with higher LHC energies.

Therefore, to address the SUSY-parameter dependence and to study the impact of bottom-quark-induced sbottom-pair production, we consider two different scenarios that are within the reach of the Tevatron and the early LHC phase. As we did in the main body of the paper, we use stop and sbottom masses of 100 (200) GeV at the Tevatron and 100 (400) GeV at the LHC, respectively, and present results for various choices of the mixing angle and the light-flavour squark and gluino masses, see Table 6. Note that

SPS1a'	$\sigma_{\text{NLO+NLL}}$ [pb]	
	LHC @ 7 TeV	LHC @ 14 TeV
$\tilde{t}_1\bar{\tilde{t}}_1$	0.379	3.71
$\tilde{t}_2\bar{\tilde{t}}_2$	1.48×10^{-2}	0.268
$\tilde{b}_1\bar{\tilde{b}}_1$	4.23×10^{-2}	0.611
$\tilde{b}_2\bar{\tilde{b}}_2$	2.51×10^{-2}	0.405

Table 5: NLO+NLL SUSY-QCD cross sections for stop and sbottom pair production at the LHC for the SPS1a' benchmark scenario. The MSTW pdfs have been adopted and the scale has been set to the mass of the particles produced.

the NLL resummation only depends on the final-state particle mass. The dependence on the other SUSY parameters enters exclusively through the NLO virtual corrections. The numbers listed in Table 6 reveal that the dependence of the cross section on the mixing angle, the gluino mass, and the light-flavour squark masses is small indeed, with variations of at most 2% both at the Tevatron and at the LHC.

$$\sigma(pp/p\bar{p} \rightarrow \tilde{t}_1 \bar{\tilde{t}}_1) \text{ [pb]}$$

	Tevatron (1.96 TeV)		LHC @ 7 TeV		LHC @ 14 TeV	
	100	200	100	400	100	400
$m_{\tilde{t}_1}$ [GeV]	100	200	100	400	100	400
SPS1a' default	15.9	0.253	423	0.218	1.77×10^3	2.34
$\sin 2\theta_{\tilde{t}} = -1$	15.9	0.255	425	0.222	1.78×10^3	2.39
0	15.9	0.254	423	0.219	1.77×10^3	2.36
+1	15.9	0.253	423	0.218	1.77×10^3	2.33
$m_{\tilde{g}} = 200$ GeV	15.8	0.248	423	0.217	1.77×10^3	2.34
500 GeV	15.9	0.252	423	0.218	1.77×10^3	2.34
1000 GeV	15.9	0.255	423	0.219	1.77×10^3	2.34
$m_{\tilde{g}} = 200$ GeV	15.8	0.251	421	0.214	1.76×10^3	2.29
500 GeV	15.9	0.253	423	0.217	1.77×10^3	2.33
1000 GeV	15.9	0.254	424	0.219	1.77×10^3	2.34

Table 6: The NLO+NLL cross sections for stop-antistop production at the Tevatron and the LHC. We compare the SPS1a' default input for the stop mixing angle and the light-flavour squark and gluino masses with various other choices for these SUSY parameters. Note that only one parameter is changed at a time, while the others are kept at their default values. The MSTW pdfs have been adopted and the scale has been set to the final-state stop mass.

Cross sections for $\tilde{b}_1 \bar{\tilde{b}}_1$ production are collected in Table 7. We compare the LO bottom-quark-induced contributions with the LO and NLO+NLL predictions based on the stop-like contributions that exclude bottom-quark initial states. Using the notation introduced in Sect. 2 and $m_-^2 \equiv m_{\tilde{g}}^2 - m_{\tilde{b}_1}^2$, the LO bottom-quark-induced contributions read

$$\sigma_{b\bar{b} \rightarrow \tilde{b}_1 \bar{\tilde{b}}_1}^{(0)} = \frac{\alpha_s^2 \pi C_F}{N_c s} \left[\left(\frac{m_{\tilde{g}}^2 s [1 - \cos(4\theta_{\tilde{b}})]}{8(m_{\tilde{g}}^2 s + m_-^4)} - \frac{s + 2m_{\tilde{b}_1}^2}{3s} - \frac{1 + \cos(4\theta_{\tilde{b}})}{4} + \frac{s + 2m_-^2}{2N_c s} \right) \beta \right. \\ \left. + \left(\frac{m_-^4 + sm_{\tilde{g}}^2}{N_c s^2} - \frac{(s + 2m_-^2)[3 + \cos(4\theta_{\tilde{b}})]}{8s} \right) \log \left(\frac{1 - \beta + 2m_-^2/s}{1 + \beta + 2m_-^2/s} \right) \right].$$

As these contributions depend on the gluino mass, we give results for $m_{\tilde{g}} = 200, 500$ GeV and 1 TeV. From the numbers presented in Table 7 it is clear that the $b\bar{b} \rightarrow \tilde{b}_1 \bar{\tilde{b}}_1$ channel is always strongly suppressed, with cross sections well below 1% of the stop-like contributions.

$$\sigma(pp/p\bar{p} \rightarrow \tilde{b}_1 \bar{\tilde{b}}_1) \text{ [pb]}$$

	Tevatron (1.96 TeV)		LHC @ 7 TeV		LHC @ 14 TeV	
	100	200	100	400	100	400
$m_{\tilde{b}_1}$ [GeV]						
SPS1a' default						
NLO+NLL	15.9	0.253	423	0.218	1.77×10^3	2.34
LO	12.6	0.227	305	0.156	1.35×10^3	1.67
LO $b\bar{b}$ -channel only	0.404×10^{-2}	0.330×10^{-4}	0.275	0.346×10^{-3}	1.40	0.564×10^{-2}
LO $b\bar{b}$ -channel only						
with $m_{\tilde{g}}=200$ GeV	0.986×10^{-2}	0.870×10^{-4}	0.659	0.667×10^{-3}	3.35	0.111×10^{-1}
500 GeV	0.454×10^{-2}	0.399×10^{-4}	0.309	0.408×10^{-3}	1.58	0.665×10^{-2}
1000 GeV	0.335×10^{-2}	0.220×10^{-4}	0.227	0.220×10^{-3}	1.16	0.360×10^{-2}

Table 7: The LO and NLO+NLL cross sections for sbottom-antisbottom production at the Tevatron and the LHC. We compare the default SPS1a' prediction for the stop-like contributions with the LO contributions induced by bottom-quark initial states. The MSTW pdfs have been adopted and the scale has been set to the final-state sbottom mass.

Bottom-quark-induced t -channel gluino exchange also leads to $\tilde{b}_1 \tilde{b}_1$ and $\bar{\tilde{b}}_1 \bar{\tilde{b}}_1$ final states. The LO cross section for these processes is given by

$$\begin{aligned} \sigma_{bb \rightarrow \tilde{b}_1 \tilde{b}_1}^{(0)} = & \frac{\alpha_s^2 \pi C_F}{N_c s} \left[\left(\frac{1 - N_c}{8N_c} [1 - \cos(4\theta_{\tilde{b}})] + \frac{2m_{\tilde{g}}^2 s - m_-^4 + (2m_{\tilde{g}}^2 s + m_-^4) \cos(4\theta_{\tilde{b}})}{8(m_-^4 + m_{\tilde{g}}^2 s)} \right) \beta \right. \\ & \left. + \left(\frac{m_-^4 (1 - \cos(4\theta_{\tilde{b}})) + 4sm_{\tilde{g}}^2}{4N_c s(s + 2m_-^2)} - \frac{(s + 2m_-^2)(1 - \cos(4\theta_{\tilde{b}}))}{8s} \right) \log \left(\frac{1 - \beta + 2m_-^2/s}{1 + \beta + 2m_-^2/s} \right) \right], \end{aligned}$$

with the identical expression for the charge conjugate process $\bar{b}\bar{b} \rightarrow \bar{\tilde{b}}_1 \bar{\tilde{b}}_1$. The corresponding numerical results for $\tilde{b}_1 \tilde{b}_1$ production are listed in Table 8. Also the $\tilde{b}_k \tilde{b}_k$ and $\bar{\tilde{b}}_k \bar{\tilde{b}}_k$ processes are suppressed by the small bottom-quark pdfs and never exceed the per-mille level with respect to $\tilde{b}_k \bar{\tilde{b}}_k$ production.

$$\sigma(pp/p\bar{p} \rightarrow \tilde{b}_1\tilde{b}_1) \text{ [pb]}$$

$m_{\tilde{b}_1}$ [GeV]	Tevatron (1.96 TeV)		LHC @ 7 TeV		LHC @ 14 TeV	
	100	200	100	400	100	400
SPS1a' default	0.111×10^{-2}	0.188×10^{-4}	0.716×10^{-1}	0.205×10^{-3}	0.362	0.306×10^{-2}
$m_{\tilde{g}} = 200$ GeV	0.568×10^{-2}	0.518×10^{-4}	0.335	0.242×10^{-3}	1.64	0.376×10^{-2}
500 GeV	0.157×10^{-2}	0.247×10^{-4}	0.994×10^{-1}	0.234×10^{-3}	0.500	0.349×10^{-2}
1000 GeV	0.447×10^{-3}	0.846×10^{-5}	0.297×10^{-1}	0.124×10^{-3}	0.153	0.187×10^{-2}

Table 8: The LO cross sections for $\tilde{b}_1\tilde{b}_1$ production at the Tevatron and the LHC. The MSTW pdfs have been adopted and the scale has been set to the final-state sbottom mass.

References

- [1] Yu. A. Golfand and E. P. Likhtman, JETP Lett. **13**, 323 (1971) [Pisma Zh. Eksp. Teor. Fiz. **13**, 452 (1971)].
- [2] J. Wess and B. Zumino, Nucl. Phys. B **70** (1974) 39.
- [3] W. Beenakker, M. Krämer, T. Plehn, M. Spira and P. M. Zerwas, Nucl. Phys. B **515** (1998) 3 [arXiv:hep-ph/9710451].
- [4] J. R. Ellis and S. Rudaz, Phys. Lett. B **128** (1983) 248.
- [5] LEPSUSYWG, ALEPH, DELPHI, L3, and OPAL experiments, note LEPSUSYWG/04-02.1 (<http://lepsusy.web.cern.ch/lepsusy/Welcome.html>).
- [6] A. Heister *et al.* [ALEPH Collaboration], Phys. Lett. B **537** (2002) 5 [arXiv:hep-ex/0204036].
- [7] V. M. Abazov *et al.* [D0 Collaboration], Phys. Rev. Lett. **97** (2006) 171806 [arXiv:hep-ex/0608013].
- [8] T. Aaltonen *et al.* [CDF Collaboration], Phys. Rev. D **76** (2007) 072010 [arXiv:0707.2567 [hep-ex]].
- [9] V.M. Abazov *et al.* [D0 Collaboration] Phys. Lett. B **665** (2008) 1 [arXiv:0803.2263 [hep-ex]].
- [10] V. M. Abazov *et al.* [D0 Collaboration], Phys. Lett. B **675** (2009) 289 [arXiv:0811.0459 [hep-ex]].
- [11] T. Aaltonen *et al.* [CDF Collaboration], arXiv:1005.3600 [hep-ex].
- [12] G. Aad *et al.* [The ATLAS Collaboration], arXiv:0901.0512 [hep-ex].
- [13] G. L. Bayatian *et al.* [CMS Collaboration], J. Phys. G **34** (2007) 995.
- [14] H. P. Nilles, Phys. Rept. **110** (1984) 1.
- [15] H. E. Haber and G. L. Kane, Phys. Rept. **117** (1985) 75.
- [16] D. Berdine and D. Rainwater, Phys. Rev. D **72** (2005) 075003 [arXiv:hep-ph/0506261].
- [17] G. Bozzi, B. Fuks and M. Klasen, Phys. Rev. D **72** (2005) 035016 [arXiv:hep-ph/0507073].
- [18] G. L. Kane, A. A. Petrov, J. Shao and L. T. Wang, arXiv:0805.1397 [hep-ph].
- [19] J. Hubisz, J. Lykken, M. Pierini and M. Spiropulu, Phys. Rev. D **78** (2008) 075008 [arXiv:0805.2398 [hep-ph]].
- [20] H. K. Dreiner, M. Krämer, J. M. Lindert and B. O’Leary, JHEP **1004** (2010) 109 [arXiv:1003.2648 [hep-ph]].
- [21] W. Hollik, M. Kollar and M. K. Trenkel, JHEP **0802** (2008) 018. [arXiv:0712.0287 [hep-ph]].
- [22] M. Beccaria, G. Macorini, L. Panizzi, F. M. Renard and C. Verzegnassi, Int. J. Mod. Phys. A **23** (2008) 4779 [arXiv:0804.1252 [hep-ph]].
- [23] see <http://www.thphys.uni-heidelberg.de/~plehn/prospino/> or <http://people.web.psi.ch/spira/prospino/>
- [24] W. Beenakker, R. Höpker, M. Spira and P. M. Zerwas, Nucl. Phys. B **492** (1997) 51 [arXiv:hep-ph/9610490].
- [25] A. Kulesza and L. Motyka, Phys. Rev. Lett. **102** (2009) 111802 [arXiv:0807.2405 [hep-ph]].

- [26] U. Langenfeld and S. O. Moch, Phys. Lett. B **675** (2009) 210. [arXiv:0901.0802 [hep-ph]].
- [27] A. Kulesza and L. Motyka, Phys. Rev. D **80** (2009) 095004 [arXiv:0905.4749 [hep-ph]].
- [28] M. Beneke, P. Falgari and C. Schwinn, Nucl. Phys. B **828** (2010) 69 [arXiv:0907.1443 [hep-ph]].
- [29] M. Beneke, P. Falgari and C. Schwinn, arXiv:1001.4627 [hep-ph].
- [30] W. Beenakker, S. Brensing, M. Krämer, A. Kulesza, E. Laenen and I. Niessen, JHEP **0912** (2009) 041 [arXiv:0909.4418 [hep-ph]].
- [31] S. Catani, M. L. Mangano and P. Nason, JHEP **9807** (1998) 024 [arXiv:hep-ph/9806484].
- [32] S. Catani, M. L. Mangano, P. Nason, C. Oleari and W. Vogelsang, JHEP **9903** (1999) 025 [arXiv:hep-ph/9903436].
- [33] D. de Florian, A. Kulesza and W. Vogelsang, JHEP **0602** (2006) 047 [arXiv:hep-ph/0511205].
- [34] D. de Florian and W. Vogelsang, Phys. Rev. D **71**, 114004 (2005) [arXiv:hep-ph/0501258].
- [35] D. de Florian and W. Vogelsang, Phys. Rev. D **76**, 074031 (2007) [arXiv:0704.1677 [hep-ph]].
- [36] N. Kidonakis and R. Vogt, Phys. Rev. D **68** (2003) 114014 [arXiv:hep-ph/0308222].
- [37] A. Banfi and E. Laenen, Phys. Rev. D **71** (2005) 034003 [arXiv:hep-ph/0411241].
- [38] R. Bonciani, S. Catani, M. L. Mangano and P. Nason, Nucl. Phys. B **529**, 424 (1998) [arXiv:hep-ph/9801375].
- [39] N. Kidonakis and G. Sterman, Nucl. Phys. B **505** (1997) 321 [arXiv:hep-ph/9705234].
- [40] N. Kidonakis, E. Laenen, S. Moch and R. Vogt, Phys. Rev. D **64** (2001) 114001 [arXiv:hep-ph/0105041].
- [41] S. Moch and A. Vogt, JHEP **0904** (2009) 081 [arXiv:0902.2342 [hep-ph]].
- [42] G. Grunberg, arXiv:0910.3894 [hep-ph].
- [43] R. Akhoury, M. G. Sotiropoulos and G. Sterman, Phys. Rev. Lett. **81**, 3819 (1998) [arXiv:hep-ph/9807330].
- [44] R. Akhoury and M. G. Sotiropoulos, arXiv:hep-ph/0304131.
- [45] E. Laenen, J. Smith and W. L. van Neerven, Nucl. Phys. B **369** (1992) 543.
- [46] S. Catani, M. L. Mangano, P. Nason and L. Trentadue, Nucl. Phys. B **478** (1996) 273 [arXiv:hep-ph/9604351].
- [47] MSTW, private communication: parton distribution function with improved accuracy in the evolution at large x , based on the MSTW parametrization at the input scale [48].
- [48] A. D. Martin, W. J. Stirling, R. S. Thorne and G. Watt, Eur. Phys. J. C **63** (2009) 189 [arXiv:0901.0002 [hep-ph]].
- [49] A. Vogt, Comput. Phys. Commun. **170** (2005) 65 [arXiv:hep-ph/0408244], see <http://www.liv.ac.uk/~avogt/pegasus.html>
- [50] A. Kulesza, G. Sterman and W. Vogelsang, Phys. Rev. D **66** (2002) 014011 [arXiv:hep-ph/0202251].
- [51] J. A. Aguilar-Saavedra *et al.*, Eur. Phys. J. C **46** (2006) 43 [arXiv:hep-ph/0511344].

- [52] C. Amsler *et al.* [Particle Data Group], “Review of particle physics,” Phys. Lett. B **667** (2008) 1 and 2009 partial update for the 2010 edition.
- [53] W. Porod, Comput. Phys. Commun. **153** (2003) 275 [arXiv:hep-ph/0301101].
- [54] P. M. Nadolsky *et al.*, Phys. Rev. D **78** (2008) 013004 [arXiv:0802.0007 [hep-ph]].
- [55] R. D. Ball, L. Del Debbio, S. Forte, A. Guffanti, J. I. Latorre, J. Rojo and M. Ubiali, arXiv:1002.4407 [hep-ph].
- [56] W. Beenakker, M. Krämer, T. Plehn and M. Spira, arXiv:hep-ph/9810290.